Article

A Minimal-Data Approach for Film Thickness Prediction in Tribological Contacts Using Venner's Equation

Felix Müller *, Patrick Wingertszahn, Oliver Koch and Bernd Sauer

Chair of Machine Elements, Gears and Tribology, RPTU Kaiserslautern-Landau, 67663 Kaiserslautern, Germany; patrick.wingertszahn@mv.rptu.de (P.W.); oliver.koch@rptu.de (O.K.); bernd.sauer@rptu.de (B.S.)
* Correspondence: felix.mueller@rptu.de; Tel.: +49-631-205-5058

Abstract: The accurate design of tribological contacts, such as those in bearings and gearboxes, makes them highly efficient and helps reduce emission in all driven systems. Traditionally, this process requires more lubricant data than data sheets typically provide, mainly kinematic viscosity at 40 °C and 100 °C and density, which limits the design process. This study introduces a simplified methodology for determining lubricant film thickness, one of the main design critical parameters, using minimal viscosity measurements obtained with a high-pressure viscometer. The researchers demonstrate that essential lubricant parameters can be derived effectively from a few measurements. By combining state-of-the-art models for film thickness with practical measurements from an EHL tribometer, this study confirms that reliable film thickness predictions can be made from basic viscosity data. This approach streamlines the design process, making tribological simulations more accessible and cost-effective, and enhances the design of tribological contacts under extreme conditions.

Keywords: tribology; friction; viscosity; elastohydrodynamic lubrication (EHL); rheology; high-pressure viscometers; contact calculation

1. Introduction

The behavior of a lubricant, particularly its viscosity, significantly impacts the friction and wear behavior of a tribological system [1]. Therefore, lubricants play a central role in almost all technical applications, such as bearings, gearboxes, and manufacturing technology. They are crucial for the efficiency of gearboxes and the durability of machine elements in highly strained contacts [2,3]. In these applications, lubricants are subjected to extreme conditions in the contact area, where the pressure in lubrication gaps can be up to 5 GPa [4].

Some lubricants are highly additivated, which improves certain characteristics of the lubricant formulation which the base fluid cannot provide or cannot provide to a sufficient extent. This can enhance lubricant performance under extreme conditions [5,6]. Depending on the complexity of the application, system models ranging from broad overviews to extremely detailed individual contact models and elastohydrodynamic lubrication (EHL) simulations are employed in the design process [7–11]. Consequently, reliable material data models represent a prerequisite for predictive tribological simulations, ensuring the optimal performance and longevity of the components involved [12,13].

Typically, very little is known about the properties of practical lubricants. Often, the data sheet only provides the density at 20 °C and ambient pressure, as well as kinematic viscosity at 40 °C (KV40) and 100 °C (KV100). Manufacturers do not usually measure other data. However, most models for calculating lubricant film thickness require many more input parameters, such as lubricant parameters according to Vogel [14] or FVA400 [15]. This study demonstrates that with a few measurements with a viscometer, it is possible to determine sufficient parameters to reliably calculate lubricant film thickness at low shear rates. Established assumptions and equations from current technology are utilizing established assumptions and equations from the state of the art.

2. Materials and Methods

In this work, lubricant film height was calculated for several lubricants by using a state-of-the-art approach, which normally requires a very precise and detailed knowledge of many lubricant parameters. In order to show that sufficient lubricant data can be determined for these calculations with little effort, i.e., to show that they are also economically viable for small- and medium-sized companies, the viscosity of the test lubricants was measured with a measuring device. The viscosity measurements were in the range of ambient pressure and room temperature up to 400 MPa and 100 °C. The measurements were performed on a high-pressure viscometer presented in [16]. It was built by Bair [17] and further developed at MEGT, allowing measurements up to 10^5 mPa · s. The quality of the results was confirmed on the basis of the measured lubricant film heights. Measurements were carried out on an EHL tribometer for this purpose. The results are presented in Section 3 and subsequently discussed in Section 4.

2.1. Viscometer

In the viscometer (shown in Figure 1), pressure is generated by using a combination of devices, including a hydraulic press, a low-pressure cylinder, a high-pressure cylinder, and a pressure regulator connected to a high-pressure test chamber. Di(2-ethylhexyl) is utilized as the pressure-transmitting fluid. The applied pressure is directly measured within the pressurized fluid by using a pressure transducer.

The high-pressure section contains a pressure vessel sealed by a viscometer plug featuring a Bridgman seal. This seal consists of a plug piston with a threaded stem, two unhardened tool steel back-up rings, and glass fiber-reinforced TFE and rubber packing. The packing is compressed through a threaded mechanism, ensuring a tight seal. Inside the pressure vessel, there is a thin-walled tube, which is closed on one end with a plug and on the other end with a movable cylinder. This cylinder equalizes the pressure, ensuring that the fluid sample in the tube experiences the same pressure as the vessel.
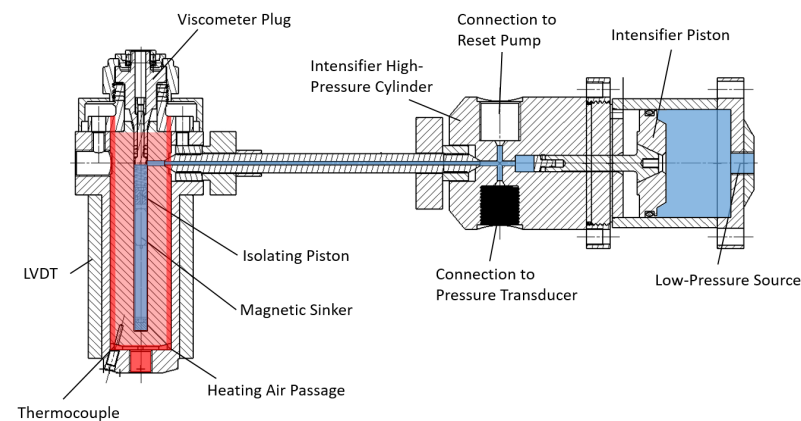

Figure 1. The structure of the high-pressure viscometer. The left part represents the actual measuring device. The right part includes a piston to induce pressure. The hot air ducts are shown in dark red, and the heated test volume is marked in light red [16].

The fluid sample is loaded into the tube, followed by the insertion of a sinker. The metallic sinker is magnetic, allowing its motion to be detected by a linear variable differential transformer (LVDT). Two types of sinkers can be used: one optimized for low-viscosity measurements (sinker 1—hollow) and another suitable for high-viscosity measurements (sinker 2—solid). The movement of the sinker within the LVDT generates a voltage signal, which is proportional to the falling speed v of the sinker. By using Equation (1), the viscosity can be determined from the speed, the density of the sinker, and the density of the fluid.

$$\eta(p, \vartheta) = C(\vartheta) \cdot v \cdot \frac{\rho_{\text{sinker}} - \rho_{\text{fluid}}(p, \vartheta)}{\rho_{\text{sinker}}} \tag{1}$$

In this Equation, ϑ is the temperature, v is the falling speed, p is the pressure, and C is a calibration variable that is a function of the temperature (3). The density of the sinker ρ_{sinker} is known, while the density of the fluid ρ_{fluid}, as is often the case in lubricant data sheets, is only provided for 15 °C. However, the density of the fluid also depends on temperature and pressure and therefore needs to be measured within the specific pressure and temperature range for accurate viscosity determination. This measurement cannot be performed with the viscometer used. Consequently, the density change was estimated by using reference oils from [15,18]. Oils with similar base oil types were used as references for the lubricant parameters. With the respective reference density $\rho_{0,\text{fluid}}$ and the associated density–temperature coefficient $\alpha_{\rho,\vartheta}$, given in Table 1, the density $\rho_{\text{fluid}}(p, \vartheta)$ can be determined by using Equation (2).

$$\rho_{\text{fluid}}(p, \vartheta) = \rho_{0,\text{fluid}}(p) + \alpha_{\rho,\vartheta} \cdot (\vartheta - \vartheta_0) \tag{2}$$

Table 1. Values for the reference density and the associated density–temperature coefficient according to [15].

	Lubricant A	**Lubricant B**	**Lubricant C**
$\rho_0/\text{g/mL}$	0.8776	0.8382	0.8382
$\alpha_{\rho,\vartheta} /\text{g/(mL·°C)}$	-6.00×10^{-4}	-6.00×10^{-4}	-6.00×10^{-4}

The calibration variables shown in Table 2 characterize the geometry of the experimental setup, i.e., the influence of the geometry of the falling body and the sample tube on the falling velocity and the flow field.

$$C(\vartheta) = C_0 + C_1 \cdot \vartheta \tag{3}$$

The temperature ϑ is given here in °C.

Table 2. The calibration variables of the two falling bodies used.

	Sinker 1—Solid	**Sinker 2—Hollow**
C_0 [1]$/\text{mPa·s/s}$	41.7	4186
C_1 [1]$/\text{mPa·s/s/°C}$	-0.033	-7.25

[1] Calibration was performed by using tri(2-ethylhexyl)trimellitate [17] and di(2-ethylhexyl)sebacate [19], [1] data.

The velocity is evaluated in the stationary range of the fall time of the sinker. Figure 2 shows an exemplarily taken measurement signal.

The blue dots indicate the position of the sinker falling from the top to the bottom position. After reaching the bottom position, the viscometer is turned over, and the sinker falls back to its initial position. To determine the falling velocity, a tangent is fitted to the blue curve. The gradient of this fit is considered the stationary falling velocity v in Equation (1). With very-low-viscosity fluids, it is only possible to evaluate very few points. A measurement can take up to several hours for high-viscosity fluids.

Temperature control is achieved by supplying heated air through a pressure regulator, which is then heated by a heating cartridge located in a large tube before the regulator. The temperature is regulated by adjusting the supply voltage to the heating element and monitored by using a type J thermocouple, providing an accuracy of approximately ±0.5 °C.

In this work, measurements were carried out at temperatures of 40 °C and 100 °C for three different oils. The pressure was varied among ambient pressure 0.1 MPa, 200 MPa, and 400 MPa. For each combination of pressure and temperature, five measurements were taken to ensure repeatability. The properties according to the oil manufacturers of the examined lubricants are shown in Table 3.
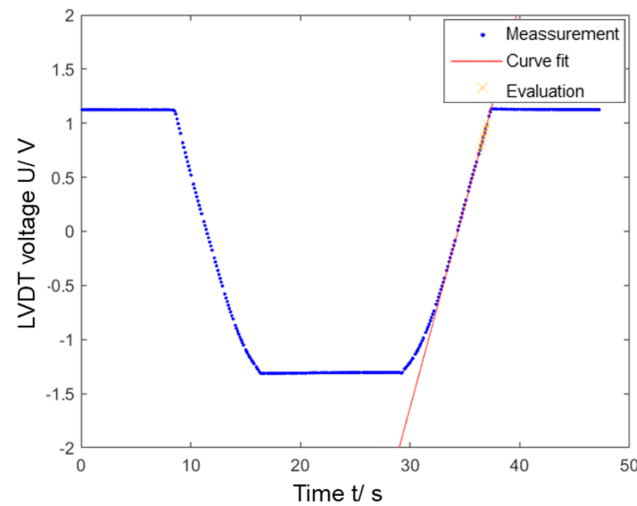
Figure 2. An example of the recorded fall curve of the sinker during viscosity measurements. Measurement signal (indicating the sinker position) as a function of the measurement time [16].

Table 3. Properties of the examined lubricants provided by the manufacturer.

	Lubricant A	Lubricant B	Lubricant C
Composition	Mineral oil + ester	PAO + mineral oil	PAO + ester
kinematic viscosity at 40 °C v_{40}/cSt	150	680	260

2.2. Determination of Viscosity Parameters

Based on the measured viscosity, there can be specific parameters determined to calculate the dynamic viscosity of a lubricant in dependence of pressure and temperature. For this calculation, Formula (4) is used according to [15]:

$$\eta(p, \vartheta) = K \cdot exp\left[\frac{B}{\vartheta + C}\right] \cdot exp\left(\frac{p}{a_1 + a_2 \cdot \vartheta + (b_1 + b_2 \cdot \vartheta) \cdot p}\right) \quad (4)$$

where again ϑ is the temperature, p the pressure, and η the dynamic viscosity. The three parameters K, B, and C are calculated by Formulas (5)–(7) according to [14]:

$$K = exp\left[ln(\eta_{40}) - \frac{ln(\eta_{100}) - ln(\eta_{40})}{-\frac{4}{13}}\right] \quad \text{in mPas} \quad (5)$$

$$B = -\frac{1755}{4} \cdot [ln(\eta_{100}) - ln(\eta_{40})] \quad \text{in } °\text{C} \quad (6)$$

$$C = 95 \quad \text{in } °\text{C} \quad (7)$$

The remaining four parameters a_1, a_2, b_1, and b_2 are determined afterwards by nonlinear regression. For this purpose, the measured viscosity values, as well as the corresponding pressure and temperature, are used, and the system of equations for the parameters is solved. With the parameters determined in this way, the viscosity can now be determined for the oils under investigation at any pressure and any temperature, which makes it possible to estimate the lubricating gap height for any operating points.

2.3. Lubricant Film Height Calculation

The measured lubricant viscosity values were then used to calculate lubricant film height in an elliptical point contact. There are several state-of-the-art approaches for this, of which Venner's equation [20] has the widest range of application, which is the

reason why this approach was used for the calculation. The following equations show this approach, starting with the calculation of the central film thickness in Equation (8):

$$H_{\text{c}} = \left[\left(\left(1.70 \cdot M^{-1/9} \cdot L^{3/4} \cdot t \right)^r + \left(1.96 \cdot M^{-1/9} \right)^r \right)^{s/r} + \left(47.3 \cdot M^{-2} \right)^s \right]^{1/s} \tag{8}$$

The dimensionless parameter for the central film thickness H_{c} is described by Equation (9).

$$H_{\text{c}} = \left(\frac{h_{\text{c}}}{R_{\text{x}}} \right) \cdot (2 \cdot U)^{-0.5} \tag{9}$$

The other parameters in Equation (8) are the dimensionless load parameter M

$$M = W \cdot (2 \cdot U)^{-3/4} \tag{10}$$

and the dimensionless material parameter L

$$L = G \cdot (2 \cdot U)^{0.25} \tag{11}$$

and the auxiliary variables r, s, and t are calculated from M and L.

$$r = exp(1 - 6/(L+8)) \tag{12}$$

$$s = 12 - 10 \cdot exp\left(M^{-2} \right) \tag{13}$$

$$t = 1 - exp\left(-0.9 \cdot \frac{M^{1/6}}{L^{1/6}} \right) \tag{14}$$

The two dimensionless parameters M and L in turn consist of the dimensionless material parameter G

$$G = \alpha_{\text{p}} \cdot E_{\text{red}} \tag{15}$$

the dimensionless velocity parameter U

$$U = \frac{\eta_0 \cdot v_{\Sigma}}{2 \cdot E_{\text{red}} \cdot R_{\text{x}}} \tag{16}$$

and the dimensionless load W

$$W = \frac{w}{E_{\text{red}} \cdot R_{\text{x}}^2} \tag{17}$$

In the above named equations, v_{Σ} is the sum velocity, E_{red} is the reduced Young's modulus of both bodies, R_{x} is the reduced radius, and w is the normal load. The determined viscosity parameters, described in Section 2.2, are necessary for the calculation of the dynamic viscosity η_0 and the pressure viscosity coefficient α_{p} used in Equations (15) and (16).
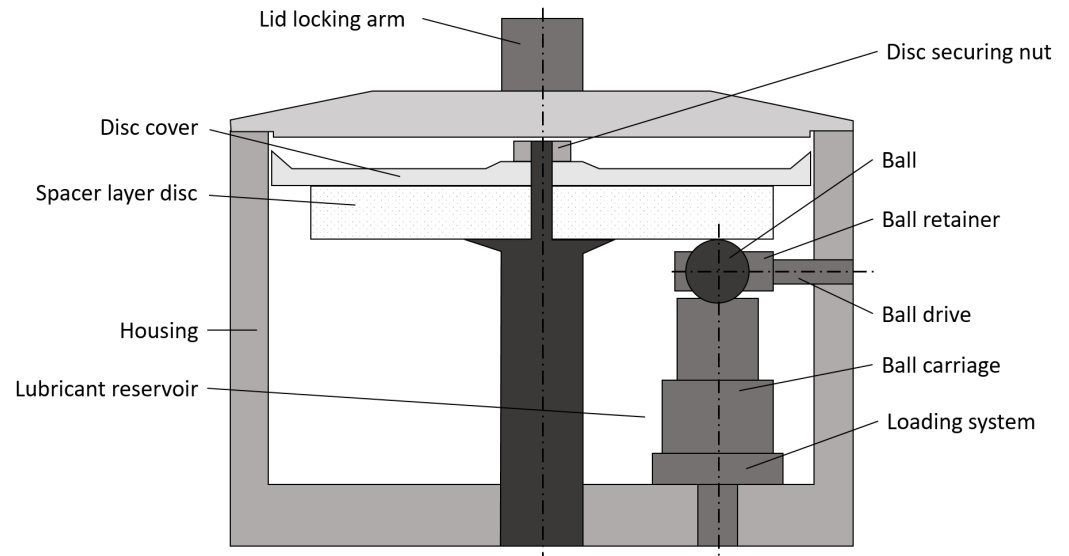
2.4. EHL Tribometer

The lubricant film thickness for an elliptical point contact was measured on the EHL tribometer "EHD-HS" by the company PCS-Instruments under different operating conditions. The EHL tribometer (shown in Figure 3) consists of a ball that is stored on a carriage consisting of three rolling bearings and a driven disc. During load application, the ball is pressed against the disc and therefore driven through the rotating disc. The tested lubricant is stored in the pot, so that half of the ball is covered in oil. Through the motion resulting from the driven disk, the lubricant is then transported in the observed point contact between ball and disc. The height of the lubricant film in direct contact is determined by using interferometry. Therefore, white light is applied on the contact through a lens, and the reflection is detected by a camera. The resulting interference is then analyzed by the software of the tribometer and evaluated into the according value for film thickness [21].

An overview over the technical specifications of the instrument is shown in Table 4.

Table 4. Technical specification of EHD-HS [21].

Test Parameter	Value
Film thickness	1 nm to 1000 nm
Load	2 to 50 N
Contact pressure	0.24 to 0.7 GPa (steel ball on glass disc)
Speeds	0.01 m/s to 20 m/s
Temperature range	Ambient to 150 °C
Test sample volume	120 mL

Figure 3. A schematic representation of the structure of the EHL tribometer in sectional view with ball disk assembly.

2.5. Lubricant Film Thickness Measurement

During the measurement of lubricant film thickness, the three lubricants stated in Table 3 were examined. The used test parameters for the measurement are stated in Table 5.

Table 5. Test parameters for ball-on-disc tribometer.

Test Parameter	Value
Speed	0.01 m/s to 2 m/s (31 data points)
Temperature	45 °C and 80 °C
Contact pressure	531 MPa

The measurements were primarily conducted at low speeds, with a speed of 0.01 m/s representing the lower limit of the measuring device. This speed is the sum speed, which consists of the sum of the disk speed and the ball speed at the contact point. There is no slip during the tests, which means that the relative speed in the contact is zero. During a measurement, the speed is then successively increased at logarithmic intervals, and a value for the central film thickness is determined at each operating point. The measurement for this is repeated a total of five times, and the result for the film thickness is derived from the mean value from the five measurements. Similar conditions were selected for the temperature as for the test on the high-pressure viscometer. The considered contact pressure of 531 MPa results from the combination of a pressure close to the typical operating conditions of lubricants and the stress limit of the glass disc of the tribometer, which is 700 MPa. A certain degree of safety was considered here, with which a realistic pressure value in typical contacts was nevertheless investigated.

In addition to that, the refractive index of the tested lubricant has to be determined, because it is a mandatory value for the calculation of film thickness with the principle of reflective interference. Therefore, the refractive index of the three lubricants was determined by using a handheld refractometer. The resulting values are presented in Table 6.

Table 6. Refractive index of examined lubricants.

	Lubricant A	Lubricant B	Lubricant C
Refractive index/−	1.4715	1.4715	1.4655

As a result of the measurement, the output file contains the investigated speeds with the corresponding measured film thickness and the exact temperature at this point. These values can then be processed to create plots with film thickness over speed and also calculate the theoretical film thickness at the exact same points by using the equations shown in Section 2.3.

3. Results

The results of the performed measurements are shown in two sections. At first, the results of the viscosity measurements from the high-pressure viscometer are shown in Section 3.1. These are then used to calculate the lubricating film thickness, which was measured with the EHL tribometer. The comparison of measured and calculated film thickness is presented in Section 3.2.

3.1. Results of Viscosity Measurements

The results of the viscosity measurements of the lubricants in Table 3 at the given operating points are shown in Figure 4. The diagram shows the dynamic viscosity of the three lubricants over the corresponding pressure at two different temperatures.
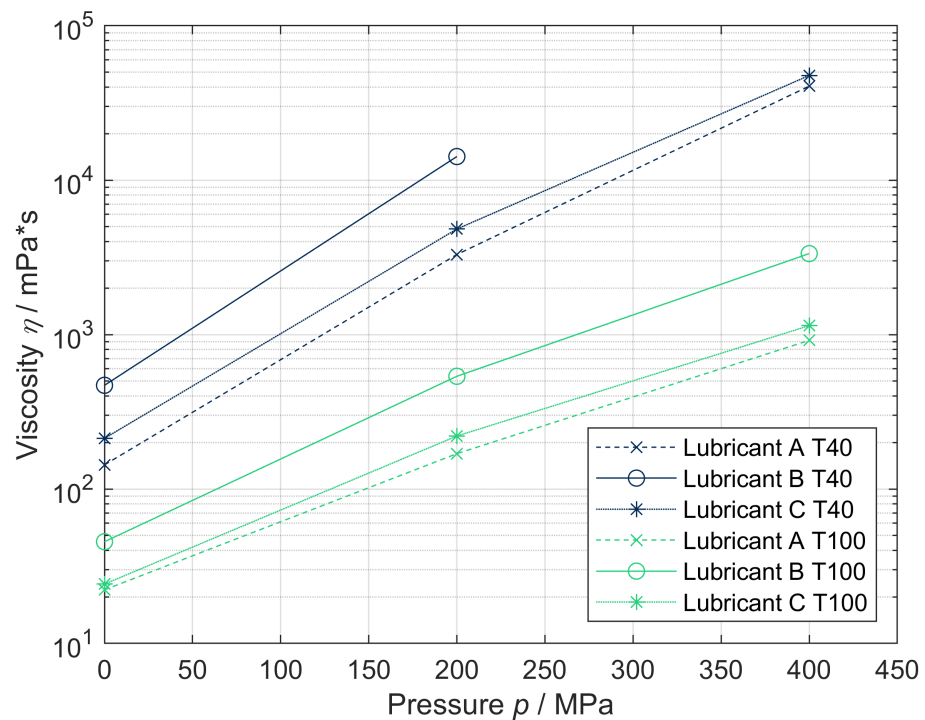

Figure 4. Results of viscosity measurements for three lubricants at different temperatures and pressures.

The results show a visible difference among the three lubricants, which is an expected behavior regarding the differences in oil composition and kinematic viscosity provided by

the producer. The missing value at a pressure of 400 MPa and a temperature of 40 °C for lubricant B can be explained by the especially high viscosity of this oil, which is out of the measuring range of the device. Therefore, the time it takes the sinker to go down inside the tube is too long to track a valid result. Every viscosity value shown in Figure 4 represents the mean value of the five measurements described in Section 2.1. The standard deviation for the performed repetitions is in a range between 0% and 5%.

3.2. Results of Film Thickness Measurements

The results of the film thickness measurements using the parameters stated in Table 5 are presented for the three lubricants in Figures 5–7. In addition to that, the theoretically determined values of the film thickness for the measured conditions are also shown. These values result from the equations shown in Section 2.3 using the lubricant parameters which where determined through the formulas in Section 2.2. The standard deviation for the performed film thickness measurements is in a range between 0 % and 5 %, similar to the viscosity measurements.
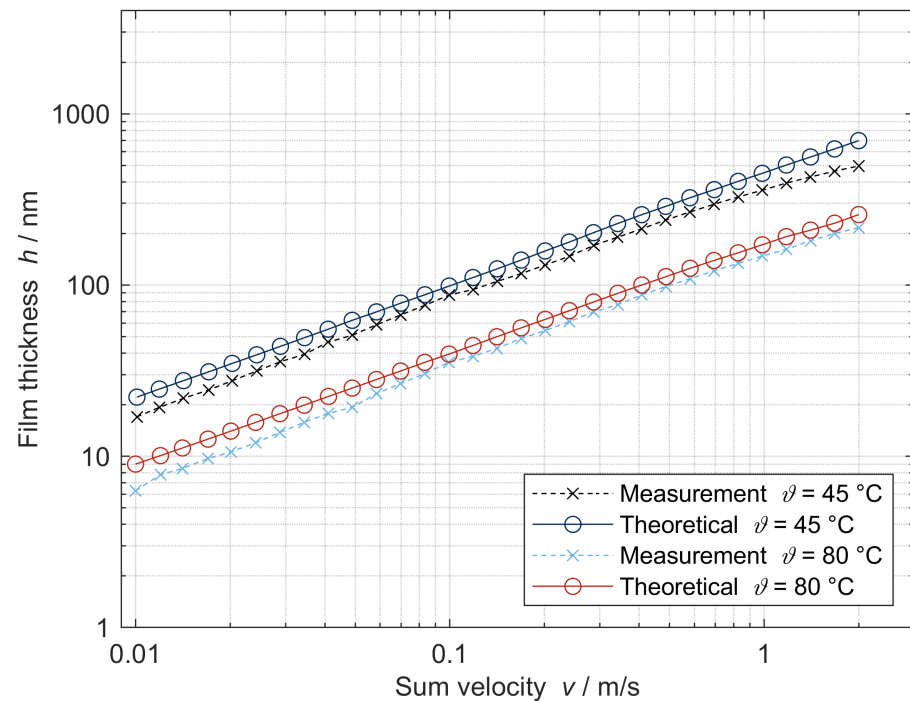

Figure 5. Results of experimentally and theoretically determined values for film thickness of lubricant A.

The calculated film thicknesses presented show very good agreement with the experimentally determined values. For lubricant A, the analytical calculation slightly overestimates the film thickness. This difference changes over the examined speeds, and the discrepancy is the lowest in the area between 0.1 m/s and 1 m/s. The increase in deviation at higher speeds can be explained by shear thinning effects, which are not accounted for in the used calculation method. In contrast to that, the calculation for lubricant B slightly underestimates the film thickness in the area of low speeds. But this behavior also changes with the increase in velocity. Overall, the analytical calculation for lubricant B fits the respective measurement slightly better than the one for lubricant A.
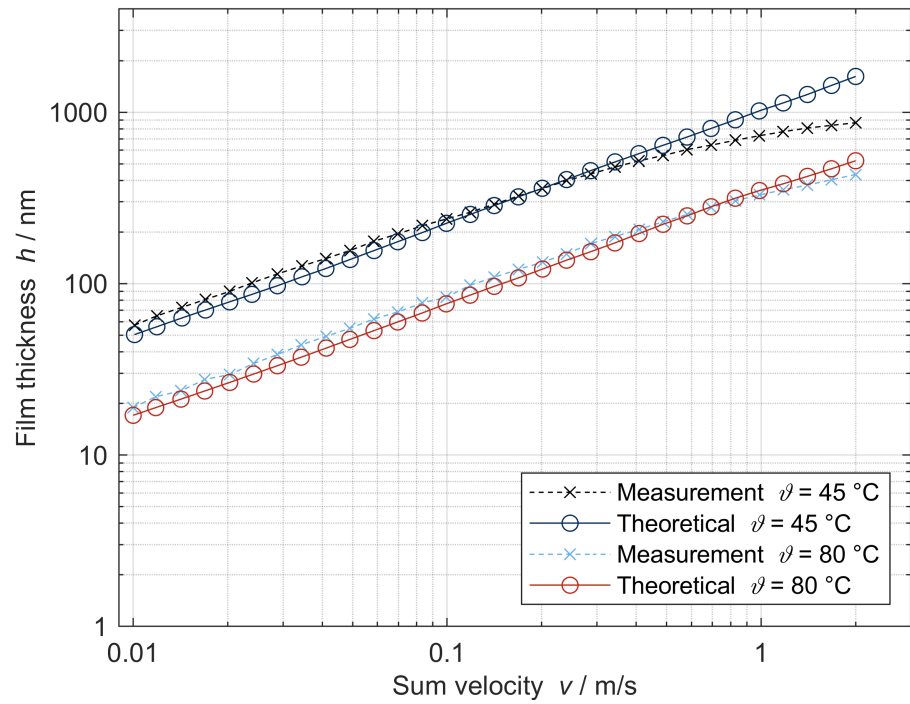
Figure 6. Results of experimentally and theoretically determined values for film thickness of lubricant B.
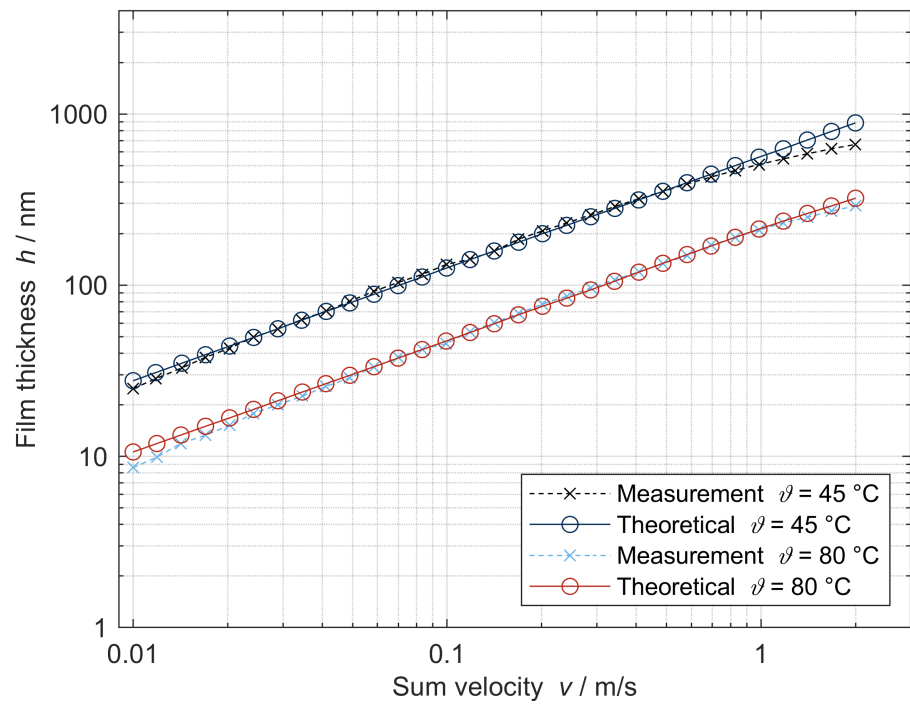

Figure 7. Results of experimentally and theoretically determined values for film thickness of lubricant C.

The results for lubricant C show a similar behavior to lubricant B but with a slight overestimation at lower speeds and a better fit with the increase in velocity. The agreement of the theoretically and experimentally determined values is even better for lubricant C than for lubricant B. The slight difference at high speed and lower temperature can be explained by the same effect as stated before. The overall lower film thickness for lubricant C is an expected result, regarding the lower viscosity compared with the one of lubricant B.

Regarding the results of the presented measurements, the determined lubricant parameters using the high-pressure viscometer show a very sufficient description of the investigated lubricants. The theoretically calculated film thickness only differs slightly from the measured results on the ball-on-disc tribometer.

4. Discussion

The lubricant film heights determined on the basis of the viscosity measurement agree very well with the measurements on the EHL tribometer. Lubricant C shows the best fit between the measured results and the analytically calculated values. The other two lubricants also show a good fit, with lubricant A having the least exact match of the three. This difference in the accuracy of the calculation can be caused by the assumptions made for the density of the lubricants to determine the viscosity.

The kinematic viscosity is not measured directly, but the falling time of a sinker in the measured fluid and the equilibrium of forces on the falling body are determined from this, and the density of the lubricant is an important input variable according to Equation (1). It was not measured here but was estimated by using a similar known fluid. This is a considerable source of error, but according to Bair, it has little influence on the quality of the measured variable for high viscosity. He stated that a difference in density of 10 leads to a relative error of the viscosity of 1 percent [17]. Since density measurements under pressure are associated with great effort, this small error is accepted for the calculation.

The input variables of the measurement itself (in this case, pressure and temperature) are also subject to a small error. They must be kept constant during the entire measurement and measured close to the fluid to be characterized. This challenge is largely overcome with the design of the measuring device. Nevertheless, small inconsistencies in temperature can be observed.

Calculating the film thickness from the measured lubricant viscosity is also a source of error. It is validated for a certain range of validity. Beyond the limits or even close to the limits, as shown in Figure 8, there may be large deviations from the measurement. The Venner approach was used in this paper, as it has the widest range of validity. Nevertheless, the equation is used here in its basic form, as published in [20]. Therefore, no additional correction factor for sheer thinning and temperature is used. This could be the main influence on the deviation between measured and calculated film thickness at high sum velocities.
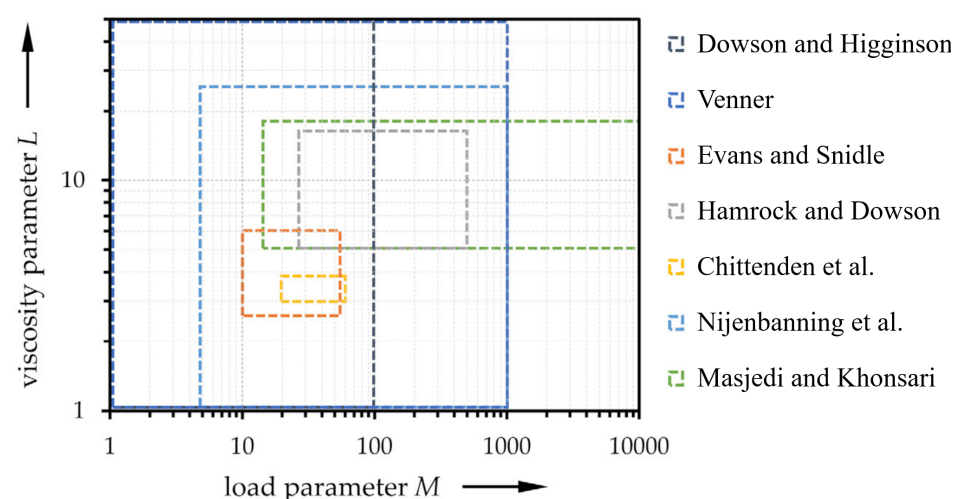

Figure 8. A qualitative comparison of the load and viscosity parameter range on which various elastohydrodynamic lubrication (EHL) film thickness equations were established for 3D point and elliptical contacts and 2D line contacts [22]. References of the compared models: Dowson and Higginson [23], Venner [24], Evans and Snidle [25], Hamrock and Dowson [26], Chittenden et al. [27], Nijenbanning et al. [28], and Masjedi and Khonsari [29].

Concerning the film thickness measurements, a possible source of error is the refractive index of the examined lubricants. It is mandatory as an input variable for the EHD-HS and determined at ambient pressure by using a refractometer. This method does not take the influence of the contact pressure on the refractive index into account, which leads to a possible error.

5. Conclusions

It was shown that lubricant film height, which is important for the design of tribological contacts, can be reliably predicted with low-input data. The basis for this is the measurement of lubricant viscosity at only a few interpolation points with the aid of a high-pressure viscometer, which was commissioned and calibrated in previous studies [16]. The assumptions made to calculate lubricant film height have proven to be valid. These are primarily the estimation of lubricant density at increased pressure and temperature by using similar reference oils, as well as the restrictions of the lubricant film height calculation according to Venner [20]. The method presented can be carried out with comparatively little effort and at low cost and delivers a very high level of accuracy. Nevertheless, due to the limitations of the measuring range of the EHL tribometer, only a pressure range up to 531 MPa could be validated. Although this can be used for tribological contacts in gears, it is far from the extreme contact pressures that occur in the rolling contacts of rolling bearings. As shown in the discussion, further studies would be necessary to show that the method can also be used reliably for this pressure range and at higher speed in contacts.

Author Contributions: Conceptualization, F.M. and P.W.; methodology, F.M. and P.W.; software, F.M.; validation, F.M.; formal analysis, F.M. and P.W.; investigation, F.M. and P.W.; resources, O.K.; data curation, F.M.; writing—original draft preparation, F.M. and P.W.; writing—review and editing, B.S.; visualization, F.M. and P.W.; supervision, O.K.; project administration, O.K.; funding acquisition, B.S. All authors have read and agreed to the published version of the manuscript.

Institutional Review Board Statement: Not applicable.

Informed Consent Statement: Not applicable.

Data Availability Statement: Data are available upon request from the authors.

Conflicts of Interest: The authors declare no conflicts of interest.

References

1. Sadinski, R.J.; Hager, C.H.J.; Hannon, W.M. A Proposed Pressure–Viscosity Coefficient Model Through Processing of Falling Body Viscometry Data for Di-(Ethylhexyl) Sebacate. *Tribol. Int.* **2023**, *145*, 011601. [CrossRef]
2. Spikes, H. Additive-additive and additive-surface interactions in lubrication. *Lubr. Sci.* **1989**, *2*, 3–23. [CrossRef]
3. Morales-Espejel, G.E.; Gabelli, A. Rolling bearing seizure and sliding effects on fatigue life. *Proc. Inst. Mech. Eng. Part J J. Eng. Tribol.* **2019**, *233*, 339–354. [CrossRef]
4. Stachowiak, G.W. How tribology has been helping us to advance and to survive. *Friction* **2017**, *5*, 233–247. [CrossRef]
5. Bhaumik, S.; Paleu, V. Wear and Rolling Contact Fatigue Analysis of AISI 52100 Bearing Steel in Presence of Additivated Lubricants. *Metals* **2021**, *11*, 907. [CrossRef]
6. Xiao, H.; Liu, S. 2D nanomaterials as lubricant additive: A review. *Mater. Des.* **2017**, *135*, 319–332. [CrossRef]
7. Wingertszahn, P.; Koch, O.; Maccioni, L.; Concli, F.; Sauer, B. Predicting Friction of Tapered Roller Bearings with Detailed Multi-Body Simulation Models. *Lubricants* **2023**, *11*, 369. [CrossRef]
8. Tošić, M.; Larsson, R.; Stahl, K.; Lohner, T. Thermal Elastohydrodynamic Analysis of a Worm Gear. *Machines* **2023**, *11*, 89. [CrossRef]
9. Farrenkopf, F.; Schwarz, A.; Lohner, T.; Stahl, K. Analysis of a Low-Loss Gear Geometry Using a Thermal Elastohydrodynamic Simulation including Mixed Lubrication. *Lubricants* **2022**, *10*, 200. [CrossRef]

10. Kramer, V.; Atalay, O.; Rüth, L.; Wingertszahn, P.; Bartz, M.; Goetz, S.; Schleich, B.; Koch, O.; Wartzack, S. Method for the consideration of statistically distributed geometrical deviations in the design of cylindrical roller bearing arrangements. *Forsch. Ingenieurwesen* **2024**, *88*, 30. [CrossRef]

11. Harris, T.A.; Kotzalas, M.N. *Rolling Bearing Analysis-2 Volume Set*; CRC Press: Boca Raton, FL, USA, 2006. [CrossRef]

12. Wingertszahn, P.; Koch, O. Vorhersage von Lagerschäden jenseits von Rolling Contact Fatigue. In Proceedings of the 6th VDI-Fachkonferenz Schadensmechanismen an Lagern, Aachen, Germany, 17–18 April 2024.

13. Wingertszahn, P.; Koch, O. Prediction of Bearing Damage Beyond Rolling Contact Fatigue. In Proceedings of the 78th Annual Meeting and Exhibition (STLE), Minneapolis, MN, USA, 19–23 May 2024.

14. Gold, P.W.; Schmidt, A.; Loos, J.; Aßmann, C. Viskosität-Temperatur-Koeffizienten von mineralischen und synthetischen Schmierölen. *Tribol. Und Schmier.* **2001**, *48*, 40–48.

15. Walbeck, T. *Schmierfilmdicke—Einfluss von Grundölart, Additivierung und Gebrauchszustand auf Viskositätsverhalten und Schmierfilmbildung. Abschlussbericht zum FVA-Forschungsvorhaben 400 (Heft 743)*; Technical Report; FVA: Frankfurt/Main, Germany, 2004.

16. Wingertszahn, P.; Schmitt, S.; Thielen, S.; Oehler, M.; Magyar, B.; Koch, O.; Hasse, H.; Stephan, S. Measurement, Modelling, and Application of Lubricant Properties at Extreme Pressures. *Tribol. Und Schmier.* **2023**, *70*, 5–12. [CrossRef]

17. Bair, S. The temperature and pressure dependence of viscosity and volume for two reference liquids. *Lubr. Sci.* **2016**, *28*, 81–95. [CrossRef]

18. Schilling, M.; Ege, R. *Referenzöle für Wälz- und Gleitlager-, Zahnrad- und Kupplungsversuche—Datensammlung für Mineralöle (FVA-Heft 180)*; Technical Report; FVA: Frankfurt/Main, Germany, 1985.

19. Kleinschmidt, R.V.; Bradbury, D.; Mark, M. *Viscosity and Density of Over Forty Lubricating Fluids of Known Composition at Pressures to 150,000 psi and Temperatures to 425 F*; ASME: New York, NY, USA, 1953.

20. Venner, C.H.; Napel, W.E. Multilevel solution of the elastohydrodynamically lubricated circular contact problem Part 2: Smooth surface results. *Wear-Int. J. Sci. Technol. Frict. Lubr. Wear* **1992**, *152*, 369–381. [CrossRef]

21. PCS-Instruments. EHD-HS Brochure. 2022. Available online: https://pcs-instruments.com/wp-content/uploads/2022/11/EHD-HS-Brochure.pdf (accessed on 16 September 2024).

22. Marian, M.; Bartz, M.; Wartzack, S.; Rosenkranz, A. Non-Dimensional Groups, Film Thickness Equations and Correction Factors for Elastohydrodynamic Lubrication: A Review. *Lubricants* **2020**, *8*, 95. [CrossRef]

23. Dowson, D.; Higginson, G.R.; Whitaker, A.V. Elasto-Hydrodynamic Lubrication: A Survey of Isothermal Solutions. *J. Mech. Eng. Sci.* **1962**, *4*, 121–126. [CrossRef]

24. Venner, C.; Wang, J.; Lubrecht, A. Central film thickness in EHL point contacts under pure impact revisited. *Tribol. Int.* **2016**, *100*, 1–6. [CrossRef]

25. Evans, H.P.; Snidle, R.W. The Isothermal Elastohydrodynamic Lubrication of Spheres. *J. Lubr. Technol.* **1981**, *103*, 547–557. [CrossRef]

26. Hamrock, B.J.; Dowson, D. Isothermal Elastohydrodynamic Lubrication of Point Contacts: Part III—Fully Flooded Results. *J. Lubr. Technol.* **1977**, *99*, 264–275. [CrossRef]

27. Chittenden, R.J.; Dowson, D.; Dunn, J.F.; Taylor, C.M.; Johnson, K.L. A theoretical analysis of the isothermal elastohydrodynamic lubrication of concentrated contacts. I. Direction of lubricant entrainment coincident with the major axis of the Hertzian contact ellipse. *Proc. R. Soc. Lond. A Math. Phys. Sci.* **1985**, *397*, 245–269. [CrossRef]

28. Nijenbanning, G.; Venner, C.; Moes, H. Film thickness in elastohydrodynamically lubricated elliptic contacts. *Wear* **1994**, *176*, 217–229. [CrossRef]

29. Masjedi, M.; Khonsari, M. On the effect of surface roughness in point-contact EHL: Formulas for film thickness and asperity load. *Tribol. Int.* **2015**, *82*, 228–244. [CrossRef]